Characterization of Urotensin-II Receptor Structural Domains Involved in the Recognition of U-II, URP, and Urantide†

Stéphane Boivin,‡,§ Laure Guilhaudis,§ Isabelle Milazzo,§ Hassan Oulyadi,§ Daniel Davoust,§ and Alain Fournier*,‡

Laboratoire d'Études Moléculaires et Pharmacologiques des Peptides (LEMPP), Institut National de la Recherche Scientifique, Université du Québec, INRS − Institut Armand-Frappier 245 boul. Hymus, Pointe-Claire (Montréal), QC, Canada, H9R 1G6, and Laboratoire de Chimie Organique et de Biologie Structurale, IFRMP 23, UMR 6014 CNRS, Université de Rouen, 76821 Mont-Saint-Aignan, France

Received January 28, 2006; Revised Manuscript Received March 22, 2006

ABSTRACT: Urotensin-II (U-II) and urotensin-II-related peptide (URP) are potent vasoconstrictors, and this action is mediated through a G protein-coupled receptor identified as UT. This receptor is expressed abundantly in the mammalian cardiovasculature, and the effects of U-II and URP can be blocked with urantide, a selective antagonist. Thus, we carried out a study with the aim to characterize the conformational arrangement of the three extracellular loops of UT as well as the transmembrane domains III and IV. Secondary structures of the synthetic receptor fragments were determined using circular dichroism (CD) spectroscopy in a variety of solvent and micelle conditions. Spectra showed that all receptor segments but not the extracellular loop I exhibited a propensity for adopting the α-helix folding. Furthermore, using surface plasmon resonance (SPR) technology, we measured the binding affinities of the ligands, U-II, URP, and urantide toward the UT extracellular segments. SPR data showed that both U-II and URP bind extracellular loops II and III with similar affinities, whereas none of these two ligands were able to interact with the extracellular loop I. Moreover, the binding of urantide was observed only with the second extracellular loop. These results imply that U-II and URP but not urantide would bind to UT according to a common pattern. Also, the correlation of the CD spectral information with the affinity data suggested that the adoption of a helical geometry in UT, by extracellular loops II and III, might be essential for favoring the binding of ligands.

Urotensin-II (U-II) is a cyclic undecapeptide (*1*) that was originally isolated from the goby urophysis (*2*). Nevertheless, isoforms of this peptide were also found in other species of fish (*3*) as well as in amphibians (*4*) and mammals (*5*). All U-II peptides share the common cyclic hexapeptide core -CFWKYC- that is structurally similar to the central region of somatostatin-14 (-FWKT-), a segment that is essential for biological activity (*1*, *6*). The cyclic segment of the U-II isopeptides is always preceded by an acidic amino acid (Asp or Glu) and followed by a hydrophobic residue (Val or Ile). On the contrary, the *N*-terminal portion of all U-II isoforms is highly variable. Interestingly, a recent report described the isolation and structure elucidation of a novel rat peptide that shares the *C*-terminal amino acid sequence with human and rat U-II (ACFWKYCV). This peptide, now designated as a U-II-related peptide (URP[1]), exhibits a high affinity toward the U-II receptor and shares the same biological actions with U-II.

The physiological role of U-II in the mammalian cardiovascular hemodynamics and vascular smooth muscle tone control is still not fully understood (*7*). Furthermore, controversial data were even reported. Thus, biological observations indicated that actions of U-II are variable. As a matter of fact, they are influenced by the type of vascular beds and blood vessel size. Moreover, U-II effects are tissue- and species-dependent (*7*−*9*). For instance, vasoconstrictor responses were observed in the rat thoracic aorta, but vasodilating effects were detected in the rat coronaries. Nevertheless, despite the heterogeneity of vascular activities, knockout of the U-II receptor gene in mice gave rise to major vascular problems, thus confirming the key role of UT in vascular homeostasis and suggesting that U-II/UT might be involved in some cardiovascular pathologies such as hypertension (*10*).

High throughput screening showed that U-II was the endogenous ligand of an orphan receptor previously known

† Financial support was obtained from the Canadian Institutes for Health Research (CIHR), the Ministère de l'Éducation du Québec, and the Région de la Haute Normandie. S.B. receives a studentship from the Fonds de la Recherche en Santé du Québec (FRSQ).

* To whom correspondence should be addressed. Tel: (514) 630-8816. Fax: (514) 630-8850. E-mail: alain.fournier@iaf.inrs.ca.

‡ Institut Armand-Frappier.

§ Université de Rouen.

[1] Abbreviations: ACN, acetonitrile; BOP, benzotriazol-1-yl-oxy-tris-(dimethylamino)-phosphonium hexafluorophosphate; CD, circular dichroism; CMC, critical micelle concentration; DIEA, diisopropylethylamine; DMF, *N*,*N*-dimethylformamide; DPC, dodecylphosphocholine; equiv, equivalent; EC, extracellular loop; EDT, ethanedithiol; Fmoc, fluorenylmethoxycarbonyl; GPCR, G protein-coupled receptor; HFIP, 1,1,1,3,3,3-hexafluoropropan-2-ol; MRE, mean residue ellipticity; MALDI-TOF, matrix assisted laser desorption ionization − time-of-flight spectroscopy; hUT, human urotensin II receptor; rUT, rat urotensin II receptor, SDS, sodium dodecyl sulfate; SPR, surface plasmon resonance; TFA, trifluoroacetic acid; TFE, 2,2,2-trifluoroethanol; TM, transmembrane domain; URP, Urotensin-II-related peptide.

10.1021/bi060190b CCC: $33.50
Published on Web 04/22/2006

as GPR14 (*11*, *12*) and currently identified as UT. The human UT receptor (hUT) isoform was characterized and appeared to be a member of the large G protein-coupled receptor family that shares a seven transmembrane helix motif (*11*, *13*). This receptor contains 389 residues and possesses two potential *N*-glycosylation sites in the *N*-terminal domain. It also exhibits one cysteine residue in the first and second extracellular loop that are postulated to participate in a disulfide bridge. Two cysteines are also present in the *C*-terminal stretch of UT, where they represent potential posttranslation sites for the addition of palmitate. This receptor shows some structural similarities with the somatostatin receptor/subtype 4 and some opioid receptors (*13*). It is predominantly expressed in cardiovascular tissues and the motor neurons of the spinal cord (*11*, *14*).

Structure−activity relationship (SAR) studies (*15*−*18*) described the pharmacophoric requirements of the UT receptor. Hence, it was showed that the *N*-terminal segment of the U-II molecule is not essential for affinity and activity but that its cyclic structure plays a key role. Moreover, it was demonstrated that only the side chains of residues of U-II Trp^7, Lys^8, and Tyr^9 are required for receptor recognition and activation (*15*, *16*). Similar studies using goby urotensin-II identified the same pharmacophores and concluded that their precise spatial orientation is crucial for the interaction with the receptor (*19*). Also, other analyses of U-II using NMR spectroscopy (*20*) showed that the residues found in the core region probably adopt a highly ordered compact conformation with the formation, on one side of the molecule, of a hydrophobic cluster created by residues Phe^7, Trp^8, and Val^{12}. It was then postulated that this cluster may interact with a hydrophobic pocket located in the UT receptor (*20*). Additionally, the NMR analysis of URP together with Ala-scan data confirmed the importance of the triad Trp-Lys-Tyr as pharmacophores and pointed out that an inverse γ-turn is also intimately associated with the biological activity of this peptide (*21*).

Using molecular homology analysis, Kinney et al. proposed the first model of the interaction U-II−rUT in 2002 (*19*). They built a molecular complex in which the lysine residue of U-II was aligned toward the Asp^{130} side chain of TM-III of UT. This structural arrangement allowed tight contacts between the receptor and the Trp, Lys, and Tyr side chains of U-II, which were found to be essential to obtain full agonist activity with the ligand. More recently, using a similar molecular homology method, Lavecchia et al. (*22*) published the 3D structure of a model of a peptidic or nonpeptidic U-II agonist−hUT complex. Their data gave information very similar to those of Kinney et al. on the putative ligand binding pocket. Photolabeling techniques provided further data on the nature of the interaction between U-II and its receptor. In point of fact, the Phe residue of U-II would be in the close vicinity of two methionines (Met^{184} and Met^{185}) located in the fourth transmembrane domain of rat UT (*23*).

The full identification of the chemical and structural pharmacophoric requirements of UT is imperative to understand the binding and activation mechanisms involved in the formation of the U-II−UT molecular complex. Hence, in the present article, we describe a study aiming at characterizing the interaction between UT and three known ligands, that is, the agonists U-II and URP as well as the antagonist urantide. This goal was attained by first analyzing, using surface plasmon resonance, the ability of the three ligands to interact with synthetic extracellular and transmembrane fragment domains of the U-II receptor and then, by correlating their affinity with their structural propensities determined with circular dichroism. Our results showed that (i) U-II and URP interact specifically with extracellular loops II and III of hUT according to a common pattern and that (ii) urantide is recognized only by extracellular loop II. Thus, SPR and CD studies revealed that the synthetic structural UT domains contained some of the conformational and chemical features essential for the binding of hU-II to hUT. Moreover, this work produced experimental evidence that the antagonist urantide exhibited a different binding mode to that of the agonists U-II and URP.

EXPERIMENTAL PROCEDURES

Materials. All amino acid derivatives were obtained from ChemImpex International (Wood Dale, IL) or Matrix Innovation, Inc. (Montreal, QC), and the coupling reagent benzotriazol-1-yl-oxy-tris(dimethylamino)-phosphonium-hexafluorophosphate (BOP) was purchased from Matrix Innovation, Inc. (Montreal, QC). The solvents (ethanol, methanol, acetonitrile (ACN), dimethylformamide (DMF), dichloromethane (DCM), and diethyl ether) were obtained from Fisher Scientific (Montreal, QC), whereas trifluoroacetic acid (TFA), phenol, ethanedithiol (EDT), and diisopropylethylamine (DIEA) were from Sigma-Aldrich (Mississauga, ON). Dodecylphosphocholine (DPC) was purchased from C/D/N Isotopes, Inc. (Pointe-Claire, QC), and trifluoroethanol (TFE) as well as hexafluoro-2-propanol (HFIP) were from Carlo Erba-SDS (Peypin, FRA). Sodium dodecyl sulfate (SDS) was purchased from Fisher Scientific (Montreal, QC). All reagents for SPR detection were purchased from BIAcore (Uppsala, SWE), including the HBS-EP buffer (0.01 M HEPES, pH 7.4, 150 mM NaCl, 3 mM EDTA, and 0.005% (v/v) surfactant P20) and sensor chips SA. The $dPEG_4$-biotin acid was obtained from Quanta BioDesign (Powell, OH), urotensin-II-related peptide (URP) from Phoenix Pharmaceuticals, Inc. (Belmont, CA), and urantide from Peptides International (Louisville, KY). Bradykinin, angiotensin II, neuropeptide Y (NPY), and IRL-1620 were synthesized in our laboratory.

Determination of the Urotensin II Receptor (UT) Topology. Two different methods, the Kyte and Doolittle hydropathy analysis plots (*24*) and the shareware HMMTOP v2.0 (*25*), were used to predict, from the primary sequence of UT (SwissProt; Q9UKP6), the location of its structural domains, such as the extracellular loops and the transmembrane helices.

Secondary Structure Prediction. The prediction of secondary structure and the determination of helicity per residue were performed using the AGADIR program (*26*). AGADIR is a prediction algorithm based on the helix/coil transition theory, which predicts the helical behavior of monomeric peptides. Calculations were performed at pH 7 and 298 K. A minimum percentage of 0.5% helicity/residue was considered to predict the presence of a helix. For EC-I, predictions were also performed using the PHD algorithm (*27*), which predicts the secondary structure (α-helix, β-strand) of proteins.

Table 1: Description of the Synthetic UT Fragments

domain	peptides	sequences[a]
EC-I	UT(110−127)	*TYVT*KEWHFGDVGCR*VLF*
EC-II	UT(182−212)	*LPVML*AMRLVRRGPKSLCLPAWGPRAHR*AYL*
EC-III	UT(281−300)	*AQYHQ*APLAPRTARIVN*YLT*
TM-III	UT(119−146)	GDVGCR*VLFGLDFLTMHASIFTLTVMSS*
TM-IV	UT(168−194)	*LLALGTWLLALLLTLPVML*AMRLVRRG
bEC-I	biotin-$(PEG)_4$−UT(110−127)	biotin-$(PEG)_4$-*TYVT*KEWHFGDVGCR*VLF*
bEC-II	biotin-$(PEG)_4$−UT(182−212)	biotin-$(PEG)_4$-*LPVML*AMRLVRRGPKSLCLPAWGPRAHR*AYL*
bEC-III	biotin-$(PEG)_4$−UT(281−300)	biotin-$(PEG)_4$-*AQYHQ*APLAPRTARIVN*YLT*
bTM-III	biotin-$(PEG)_4$−UT(119−146)	biotin-$(PEG)_4$-GDVGCR*VLFGLDFLTMHASIFTLTVMSS*
bTM-IV	biotin-$(PEG)_4$−UT(168−194)	biotin-$(PEG)_4$-*LLALGTWLLALLLTLPVML*AMRLVRRG

[a] Italic and underlined residues indicate the position of the putative transmembrane domain.

Peptide Synthesis and Cleavage. U-II and five UT fragments, corresponding to the three UT extracellular loops (EC) and transmembrane domains (TM) III and IV, were synthesized. UT peptide fragments were identified as follows: UT(110−127) or EC-I, UT(182−212) or EC-II, UT-(281−300) or EC-III, UT(119−146) or TM-III, and UT-(168−194) or TM-IV (Table 1). A solid-phase strategy combined with Fmoc chemistry methodology was used. Briefly, all peptides were assembled using a semiautomatic multireactor system. The Wang resin was used as the solid support, and the amino acids of the peptide sequences were introduced under their Fmoc-N-protected form (3 equiv). Couplings were performed in DMF in the presence of DIEA (5 equiv), and BOP (3 equiv) was the coupling reagent. Deprotection was achieved with 40% piperidine in DMF. The peptides were deprotected and cleaved from the solid support using TFA containing a mixture of ethanedithiol, phenol, and water as scavengers (92:2.5:3:2.5). The reaction was carried out for 60 min at 0 °C. Then, the solution was filtered, and the resin was washed with an equal volume of TFA. After evaporation of TFA, the remaining oily material was precipitated with diethyl ether and collected on a fritted-glass funnel. The crude material was dried under vacuum and stored at −20 °C until purification.

Peptide Modifications for SPR Study. A small amount of each peptide-resin was modified at the *N*-terminus by introducing $dPEG_4$-biotin acid as a building block. The coupling was achieved with BOP reagent in the presence of DIEA. Deprotection and cleavage of the N-biotinylated-peptide-resin were obtained as described above.

Peptide Purification and Characterization. U-II was obtained following the previously published procedure (*15*). EC-I, EC-II, EC-III, and their related biotinylated peptides were dissolved in 10% ACN in aqueous TFA (0.2%) and purified with a RP-HPLC system (Waters PrepLC500A) equipped with a model 441 absorbance detector and a Flanged MODCol FMB-1030 (250 × 21.2 mm) column packed with Phenomenex Jupiter C_{18} (300 Å, 15 μm). Flow rate was maintained at 20 mL min^{-1} and detection was at 230 nm. Peptides were eluted with a 10−50% linear gradient of ACN (10%) in aqueous TFA (0.2%). For TM-III and TM-IV, the column was rather packed with a C_4 support (300 Å, 5 μm), and the peptides were purified with a 40−80% linear gradient of ACN in aqueous TFA (0.2%) at a flow rate of 40 mL min^{-1}. Homogeneous fractions, as established using analytical HPLC, were pooled and lyophilized. Peptide molecular weight was verified using MALDI-TOF mass spectrometry (Voyager-DE, ABI, Foster City, CA), and purity was confirmed with analytical HPLC.

Immobilization of Biotinylated Peptides for SPR. Assessments of the ligand binding to UT domains were performed using a BIAcore 2000 instrument (Biacore, Inc., Piscataway, NJ) equipped with a SA sensor chip (Biacore, Inc.). SA sensor chips were coated with streptavidin and covalently immobilized onto a carboxymethylated dextran matrix. HBS-EP was used as the running buffer. According to the manufacturer's procedure, the SA chip was conditioned with three consecutive injections of 1 M NaCl in 50 mM NaOH, at a flow rate of 100 μL min^{-1}, before the immobilization of the UT fragments. Thereafter, a solution of each biotinylated-PEG_4−UT fragment, obtained by dissolving the material in the running buffer at a concentration of 100 μM, was circulated over the conditioned SA-chip. SPR assays with the biotinylated-PEG_4−UT transmembrane domains III and IV were not carried out because these peptides were poorly soluble in HBS-EP buffer. Thus, immobilization of the three biotinylated extracellular loop domains was individually performed on the SA-chip by circulating the solution at a flow rate of 10 μL min^{-1} for 5 min. The procedure was repeated three times to favor a high density of biotinylated-UT loops on the SA-chip, and each step was accompanied with a pulse of 1 M NaCl in 10 mM NaOH at a flow rate of 50 μL min^{-1}. All experiments were performed at 25 °C, and an injection of bovine serum albumin (0.1 mg mL^{-1}), at a flow rate of 5 μL min^{-1}, was used to determine nonspecific binding.

SPR Affinity Assays. Seven peptide solutions were prepared in the HBS-EP buffer, at concentrations ranging from 16 to 718 μM, to rank their binding efficacy to the extracellular domains of UT. Among these seven ligands, three are known to bind the whole UT receptor, that is, U-II (agonist), URP (agonist), and urantide (antagonist). The four other peptides, that is, bradykinin, angiotensin II, NPY, and IRL-1620 are ligands known to bind GPCRs other than UT, and they were used as controls to determine the selectivity and specificity of binding to the UT synthetic domains. All peptides were circulated onto each UT domain immobilized on the sensor chip SA for 300 s at a flow rate of 5 μL min^{-1}, followed by a 200 s dissociation phase. Regeneration of the biotinylated-UT−SA-chip surface was achieved using a short injection of 50 mM NaOH at a flow rate of 50 μL min^{-1}. Each concentration was analyzed in triplicate, and a separate flow cell, on which only biotin had been immobilized, was used as a blank to estimate the nonspecific binding to the carboxymethylated dextran chip. The K_D value of each peptide ligand was calculated with the BIAevaluation ver. 3.2 software.

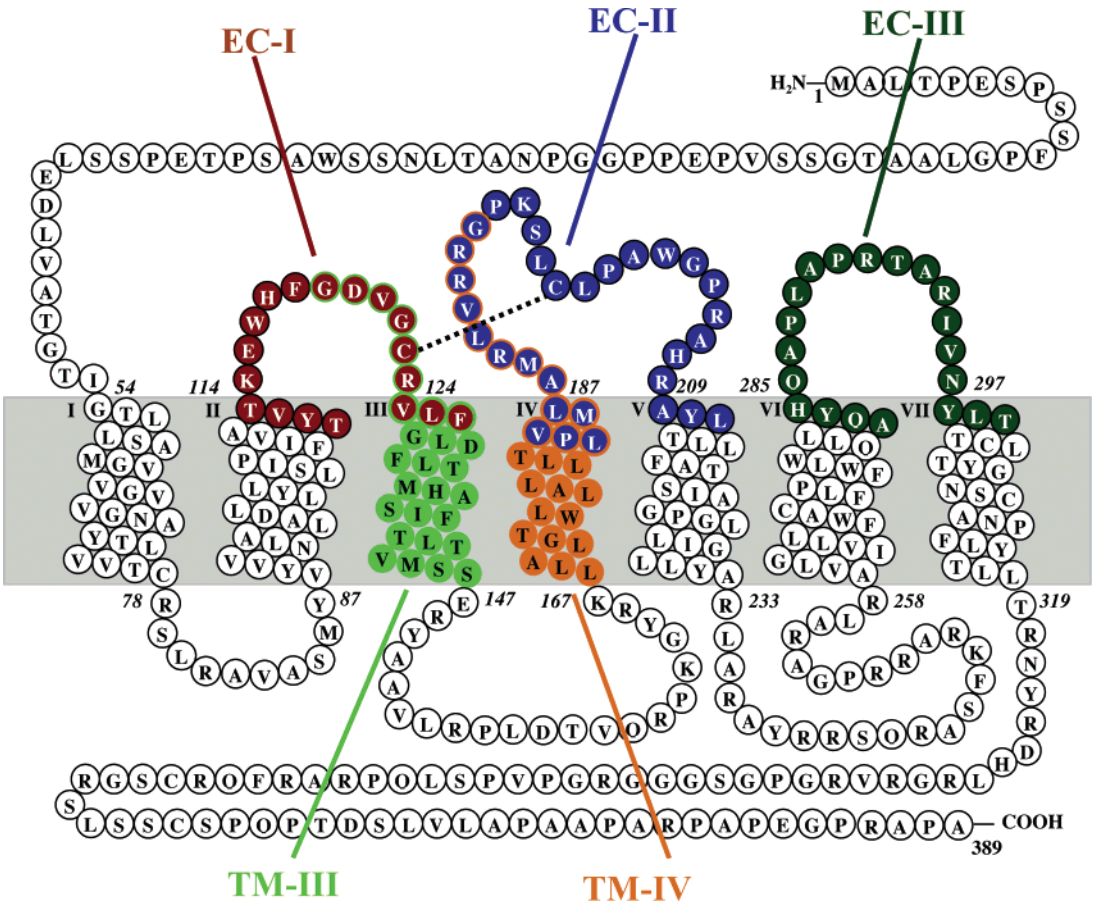

FIGURE 1: Sequence of the urotensin-II receptor (UT). The colors indicate the synthesized structural domains of UT: EC-I (extracellular loop I), EC-II (extracellular loop II), EC-III (extracellular loop III), TM-III (transmembrane domain III), and TM-IV (transmembrane domain IV).

CD Experiments. Circular dichroism spectra were recorded at room temperature from 189 to 250 nm on a CD6 dichrograph (Jobin-Yvon, Longjumeau, FRA), using quartz cells with a 0.05 cm path length. For each spectrum, 5 scans were accumulated and then averaged. The baseline was obtained by recording a spectrum of the neat solution, and it was subtracted from the peptide spectrum. Ellipticity is reported as mean residue molar ellipticity ($[\theta]_{MRE}$) in deg cm^2 $dmol^{-1}$. Three different organic solvents and two micelle-producing compounds were used at various concentrations in 10 mM phosphate buffer at pH 6.0. Those conditions were: MeOH, (30, 50, and 80%); TFE, (30, 50, and 80%); HFIP, (0.3, 3, and 25 mM); SDS (150 mM); and DPC (150 mM). The final peptide concentration was 0.1 mM, except for DPC-containing solutions for which a peptide concentration of 0.2 mM was used. The percentage of each secondary structure was evaluated using the DICHROPROT V2.6 shareware from Gilbert Deléage (CNRS Lyon, FRA).

RESULTS

Prediction of the UT Transmembrane Helical Domain Locations. The Kyte and Doolittle method was used to analyze the hydrophobic and hydrophilic tendencies of the UT primary structure (*24*). This technique gave an outline of the structure of UT in positioning the seven transmembrane domains. Afterward, the location of the helical transmembrane segments was refined with the HMMTOP v2.0 shareware (*25*) to obtain a model of UT topology (Figure 1). This model was compared to other models generated using different GPCR topology prediction methods available on the web (*28*, *29*), and very similar results were obtained with more or less 1−3 amino acid residues at the helix−loop−helix junctions.

Peptide Synthesis and Purification. U-II, the three UT extracellular loops, and UT transmembrane helices III and IV were synthesized (Table 1) using a standard Fmoc strategy. Multiple couplings and long reaction times were required to perform the synthesis of the hydrophobic transmembrane domains. For U-II and the extracellular loops, purities of ≥97% were obtained, as established by analytical HPLC. The purification of TM-III and TM-IV proved to be much more challenging because of precipitation problems. Nevertheless, TM-III and TM-IV were obtained with purities of 84 and 96%, respectively. The weak solubility of TM-III prevented us from obtaining a better purity even after an additional purification attempt. A small amount of each UT structural domain was biotinylated for SPR studies. The addition of biotin-$(PEG)_4$ at the *N*-terminus of each structural domain resulted in a slight increase of solubility for all peptides except for biotin-$(PEG)_4$−TM-III which remained poorly soluble.

Surface Plasmon Resonance Studies. The affinity and specificity of binding of different ligands toward EC-I, EC-II and EC-III were examined by SPR. Yet, transmembrane domains III and IV proved to be too hydrophobic to be diluted in the HBS-EP buffer, and therefore, the surface plasmon resonance assays were not performed. Biotinylated UT extracellular loops I, II, and III were immobilized onto

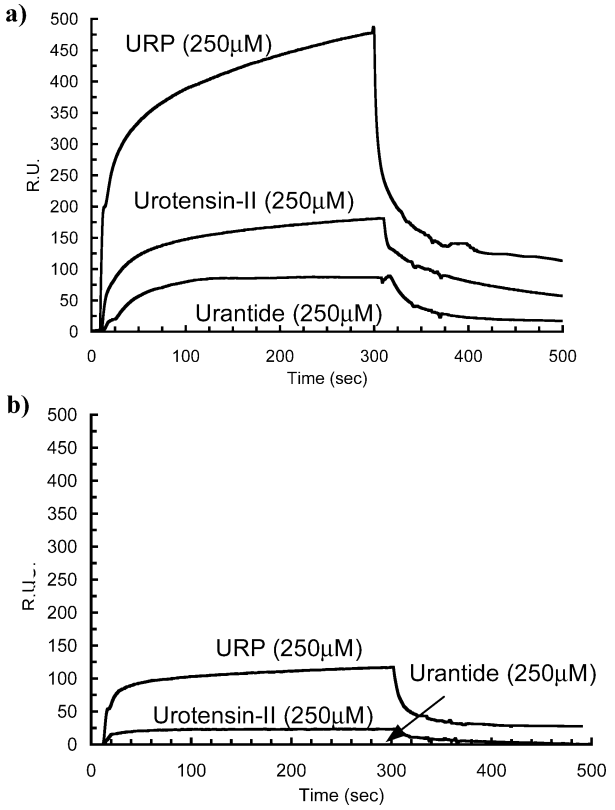

FIGURE 2: Surface plasmon resonance binding assays of U-II, URP, and urantide toward some structural domains of UT, (a) biotin-PEG_4-EC-II and (b) biotin-PEG_4−EC-III. U-II, URP, and urantide did not interact with the biotin-PEG_4−EC-I domain, and urantide did not interact with the biotin-PEG_4−EC-III domain. The lines that represent the responses of control peptides are superimposed on the baseline (angiotensin II, NPY, bradykinin, and IRL-1620).

an SA-chip by means of a strong biotin−streptavidine interaction. A high association rate combined with a low dissociation process resulted in a rapid and abundant UT domain immobilization, as shown by the strength of the SPR signal (≈1100 RU). Two agonists (U-II and URP) and one antagonist (urantide) known to bind the UT receptor were circulated over each extracellular loop domain of UT immobilized on the SA-chip, and SPR data showed that U-II, URP, and urantide interacted with some domains of UT. Hence, Figure 2a shows that U-II and URP bind to extracellular loops II and III, whereas Figure 2b demonstrates that urantide binds only to extracellular loop II. None of these three peptides interacted with extracellular loop I. In fact, the results showed that among the three ligands, URP exhibited the largest binding response on EC-II and was also more potent than U-II on EC-III. Binding on EC-II and EC-III was concentration-dependent and was rapidly reaching an equilibrium that was followed by a fast dissociation step at the end of injection. The dissociation constant (K_D) was analyzed with the BIAevaluation v.2 software from Biacore. As shown in Table 2, the peptides showed similar affinities for the EC-II and EC-III domains. Thus, U-II showed an affinity of 7.60×10^{-6} M for EC-II and 9.75×10^{-6} M for EC-III, and URP gave affinities of 1.42×10^{-6} M and 8.54×10^{-6} M for EC-II and EC-III, respectively, and finally, urantide exhibited an affinity of 2.76×10^{-6} M toward EC-II. To assess the specificity of these binding responses, four control peptides (bradykinin, angiotensin II, NPY, and IRL-1620) were evaluated in the SPR assays carried out with the structural UT domains. None of these peptides exhibited binding to EC-I, EC-II, EC-III, or the nonsubstituted surface. These results strongly suggested that the interaction of U-II, URP, and urantide with EC-II as well as that of U-II and URP with EC-III is specific.

Table 2: Affinities of U-II, URP, and Urantide toward Some UT Domains, as Determined by SPR

	EC-I K_D	EC-II K_D	EC-III K_D
U-II	n.a.[a]	7.60×10^{-6} M	9.75×10^{-6} M
URP	n.a.	1.42×10^{-6} M	8.54×10^{-6} M
urantide	n.a.	2.76×10^{-6} M	n.a.

[a] n.a.: not applicable.

Helix Structure Prediction. UT peptide sequences were submitted to the prediction program AGADIR. For the extracellular loops, no helical content was predicted for EC-I, whereas a strong helicity was proposed for the segments 183−193 and 205−210 of EC-II, and a moderate helicity was predicted between residues Pro^{290} and Tyr^{298} of EC-III. An analysis of the UT transmembrane domains with AGADIR suggested a highly stable helix for portions123−127 and 131−138 of TM-III and 171−192 of TM-IV, respectively.

Structural Studies Using Circular Dichroism. The overall CD spectrum of a given peptide/protein represents the combination of the individual spectra of each secondary structure found in the molecule. Therefore, we used CD to investigate the secondary structure content of extracellular domains I, II, and III as well as that of transmembrane domain IV of UT. CD measurements of the UT segments were carried out in a variety of media such as phosphate buffer, organic solvents (MeOH, TFE or HFIP)/buffer mixtures, and solutions containing cell membrane-mimetic micelles (SDS and DPC). A complete CD evaluation of the various domains, in all media, was not possible because of the lack of sufficient solubility that is sometimes observed with the peptides. Nonetheless, as shown in Figure 3, a set of CD data was recorded for all peptides in either stabilizing conditions.

Hence, in the phosphate buffer, EC-I showed a low solubility, but so far, its CD spectrum suggested a predominant random-coil conformation in that condition. However, upon the addition of 30% HFIP to the buffer, EC-I solubility improved, and its CD spectrum then exhibited a pattern related to a β-sheet structure, as characterized by a negative band at 218 nm and a positive signal at 196 nm. A rise of HFIP concentration from 30 to 80% led to a further stabilization of the partially folded β-sheet, as shown by a marked increase of the Cotton effect (Figure 3a). Similar conformational data were obtained in neat MeOH. Deconvolution of these spectra with DICHROPROT gave an estimate of 3% α-helix and 56% β-sheet. CD results are in accordance with PHD, which predicted a β-strand for segments 2−9 and 13−17.

The CD spectra of EC-II in phosphate buffer, displayed patterns similar to those of EC-I in the same condition. Consequently, EC-II, which is also poorly soluble, gave a CD spectrum lacking any of the features typical of canonical secondary structures. This observation showed that this peptide adopted a disordered conformation in this medium.

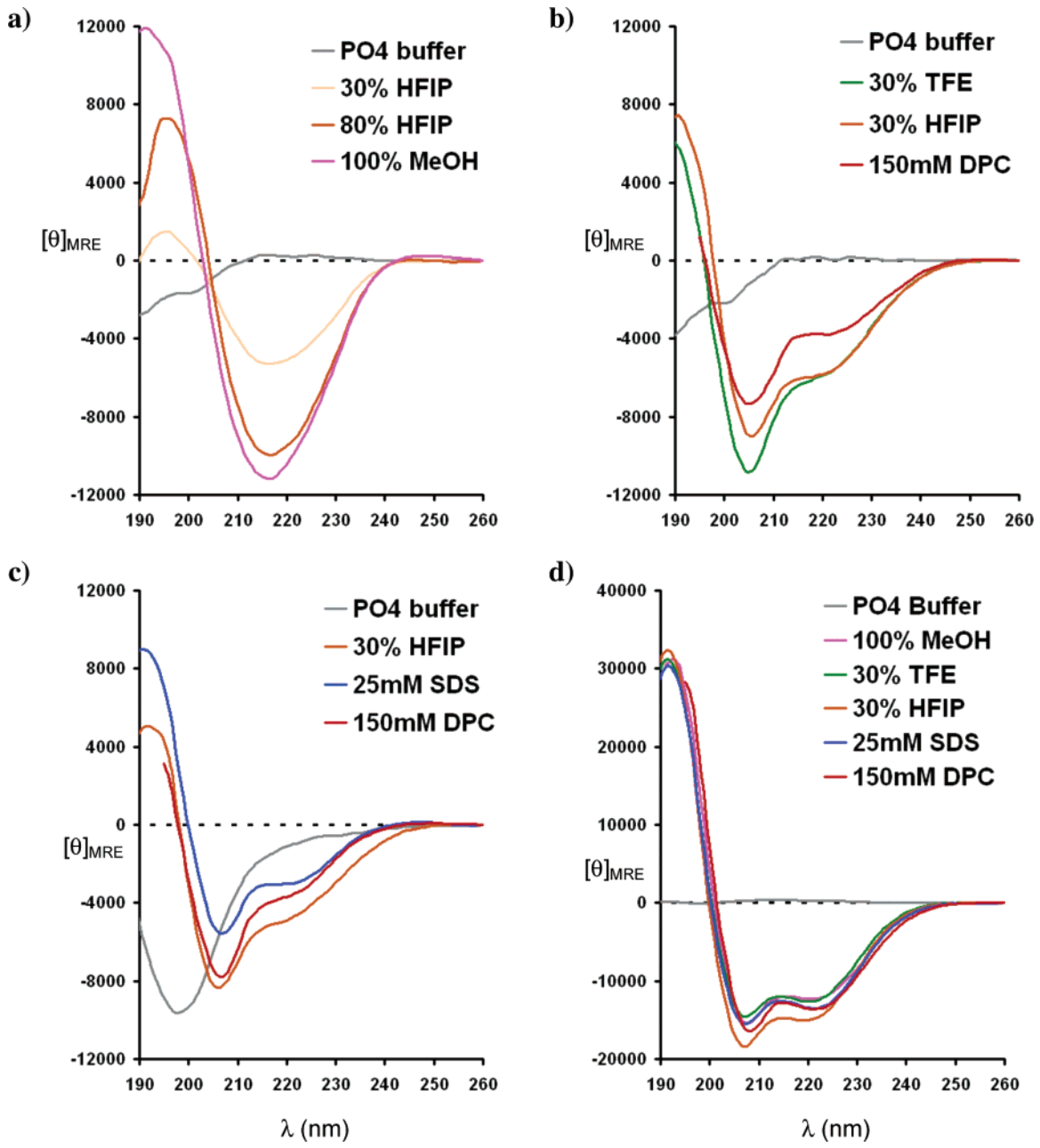

FIGURE 3: Circular dichroism (CD) spectra of (a) EC-I, (b) EC-II, (c) EC-III, and (d) TM-IV in a variety of solvents (or media). Ellipticity is reported as mean residue molar ellipticity ($[\theta]_{MRE}$) in deg cm^2 dmol^{-1}.

However, as shown in Figure 3b, in the presence of organic solvents or DPC micelles, the CD spectra exhibited two minima at 208 and 222 nm, a characteristic that is typically found with the α-helix conformation. In organic solvent/buffer mixtures, all analyzed peptides showed a higher helical content than that in a micellar DPC environment. However, when increasing the concentration of the organic solvent up to 80%, a decrease of the molar ellipticity measured at 222 nm was observed, suggesting a decrease of solubility for the peptide at higher concentrations of TFE or HFIP. Deconvolution of the spectra with DICHROPROT gave, in DPC, a helical content of 18%, corresponding to approximately 6 residues, and a helix content of about 30% in HFIP or TFE, corresponding to approximately 8−10 residues out of 31.

The CD spectrum of EC-III in phosphate buffer was characterized by a strong negative signal at 198 nm, which can be associated with a random-coil arrangement (Figure 3c). A similar spectrum was observed in neat MeOH or in the presence of TFE. However, the addition of HFIP or detergents such as SDS and DPC resulted in marked changes in the CD spectra, consistent with an increase of secondary structure content that can be correlated to an α-helix geometry, as shown by the negative Cotton effects appearing at 208 and 222 nm. Using the DICHROPROT software, the helical content can be estimated at 16% in SDS micelles, at 18% in DPC micelles, and at 22% in the HFIP solution. These percentages would correspond to 3, 4, and 5 residues out of 20, in the respective conditions.

As expected, TM-IV adopts a helical conformation in the various media as indicated by the two strong signals of mean molar ellipticity at 208 and 220 nm. These were observed in neat MeOH, 30% TFE, 30% HFIP, 25 mM SDS, and 150 mM DPC (Figure 3d). The CD spectra of TM-IV in all of these mixtures are almost identical, suggesting that the

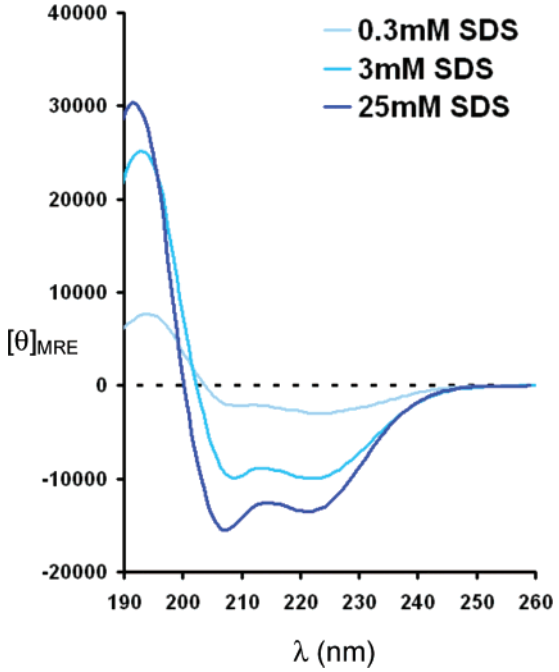

FIGURE 4: CD spectra of TM-IV of the UT receptor in the presence of increasing concentrations of SDS. The critical micellar concentration of SDS is dependent on salt concentration and is around 3.5 mM in a 10 mM phosphate buffer.

secondary structure content of this peptide is not affected by the nature of the solutes composing the medium. Using DICHROPROT, the α-helical contribution in the overall secondary structure of TM-IV was estimated to be about 50%, which would correspond to 13 residues out of 27. The effect of the SDS concentration on the TM-IV secondary structure was investigated. It can be seen from Figure 4 that in a solution containing only 0.3 mM SDS, a concentration far below the critical micellar concentration, TM-IV is weakly structured. However, around the critical micellar concentration (3 mM) as well as above (25 mM) it, the spectral features typical of the α-helix structure became very apparent. As expected, a similar amount of helical molecular arrangement was observed in 150 mM DPC micelles, a concentration far above the critical micellar concentration (1.5 mM).

DISCUSSION

Upon the binding of a ligand, GPCRs reveal a structural reorganization that leads to receptor activation and the transduction of a signal. This recognition phenomenon involving GPCRs requires the participation of different receptor domains such as the *N*-terminal segment as well as the extracellular loops and/or transmembrane helices. These receptor segments are responsible for the specificity and pharmacological profile. In fact, this was well established with studies of chimeric GPCRs (*30*). The urotensin-II receptor (UT), formerly known as GPR14, is a G protein-coupled receptor, and therefore, to study the behavior of its specific domains upon the binding of three known ligands (U-II, URP, and urantide), we applied a strategy in which the key receptor segments were individually studied. The UT extracellular loops and transmembrane stretches on which we focused were synthesized using solid-phase peptide synthesis methodology. To achieve the anchoring of the receptor segments on streptavidin (SA)-coated chips used in surface plasmon resonance technology, we coupled a biotin moiety at the *N*-terminus of each peptide. Also, to prevent potential steric hindrance problems that could occur between streptavidin and the anchored fragments and/or ligands and as an attempt to improve the solubility of the synthetic receptor domains, we introduced a $(PEG)_4$ spacer. So far, streptavidin was able to recognize the biotinylated compounds, and excellent loads of peptide were attained with extracellular loops I, II, and III. However, even with the tetraPEG spacer-arm, the solubility of transmembrane domains III and IV was too low to permit a convenient load. Nevertheless, as a first step, the affinity properties of the ligands toward the synthetic extracellular loop fragments were measured with surface plasmon resonance technology. SPR data showed that U-II and URP specifically bind to extracellular loop II, suggesting that this extracellular domain is involved in the affinity phenomenon related to these two agonists. Interestingly, Boucard et al. (*23*) have previously described, using photolabeling techniques, that two methionine residues (184 and 185) of rat UT are chemically modified upon binding and UV illumination of a U-II-derived photoprobe. These two amino acids are also found in human UT, and they are positioned at the boundary of extracellular loop II and transmembrane helix IV. Therefore, our binding data in combination with Boucard's results support the hypothesis that EC-II is a crucial receptor constituent for the binding of UT agonists.

Our study also provided information suggesting that extracellular loop III would be implicated in the U-II recognition process. Again, although measured affinities were in the μM range, both U-II and URP exhibited specific binding in the presence of the synthetic EC-III fragment. Thus, SPR results, either with EC-II or EC-III, showed in both cases affinities in the μM range. This observation suggested that the SPR conditions that were used for the analyses probably did not favor an optimized folding of the immobilized receptor fragments, a requirement for a more potent binding. This postulate is supported by the CD data that showed that the helicity in the EC-II and EC-III domains was promoted, especially in membrane-mimicking environments. Hence, it appeared that UT agonists would produce their biological effects following a common binding pattern involving EC-II and EC-III. These results support the theoretical model of Lavecchia et al. (*22*) who proposed, using a structural homology evaluation of an agonist−hUT complex, a major role for the extracellular domains in the binding of P5U, a super U-II-derived agonist of UT (*31*). Nevertheless, even though experimental and theoretical data strongly suggest the involvement of EC-II and EC-III in the binding of the U-II and URP agonists, other structural UT elements such as the Asp^{130} residue of TM-III (*19*, *22*) are probably essential for the expression of a potent affinity.

Urantide is a peptidic antagonist of UT that was described in 2003 by Patacchini et al. (*32*). We used this peptide in the SPR experiments to check its affinity toward the synthetic UT fragments. In contrast to the results obtained with agonists U-II and URP, SPR data showed that urantide bound only to the EC-II domain. This finding suggests that extracellular loop III would be important not only for the recognition process with a ligand but also for triggering the cascade of events leading to cell response. Moreover, it seems

that potent UT antagonists could be designed by developing high affinity ligands specific for EC-II. So far, the nature of the interaction of U-II or URP with the EC-II or EC-III domains as well as that of urantide with EC-II is not yet characterized. Nonetheless, SPR assays of the UT fragments, carried out with other peptides not related to urotensin II (bradykinin, angiotensin II, NPY, and IRL-1620), showed that the binding of the three UT ligands was specific. Furthermore, the binding data cannot be explained only by a physicochemical parameter such as an ionic interaction. As a matter of fact, EC-II is a peptide containing several basic residues, and therefore, it exhibits a large positive charge. Nevertheless, it was observed that among the three ligands that were analyzed, URP, a peptide with a net +1 charge, was the ligand showing the best affinity compared to that of urantide (charge 0) and U-II (charge −1). Also, URP contains only one carboxylate function that is located at the *C*-terminus, and SAR studies (*19*) demonstrated that the *C*-terminal capping of urotensin II, using amidation, had no effects on the affinity or activity. Therefore, residues able to come into close contact, for instance, through hydrophobic interactions, are present in the sequence of the EC-II peptide fragment and in the three UT ligands. Structure−activity relationship analyses (*19*) reported the importance of the aromatic residues Trp and Tyr located within the cyclic core of the members of the U-II peptide family. Hence, one of these two amino acids, or both, probably interacts with short hydrophobic strands situated in the EC-II and EC-III loops. Besides, this hypothesis is further supported by SAR and conformational data (*32*), which showed that the inversion of chirality of the Trp residue, in the analogue [Pen^5,Orn^8]-hU-II(4−11), produced a potent antagonist (urantide). Thus, the identity of the extracellular loop residues participating in this putative hydrophobic interaction remains to be established, but the second half of EC-II and the first half of EC-III, because of their inherent hydrophobicity, are probably the locations containing the key moieties.

To explore the potential molecular arrangement of UT, we carried out, using circular dichroism spectroscopy, an analysis of the secondary structure adopted by the synthetic receptor fragments in various aqueous and organic media, including cell membrane-mimicking conditions. The use of receptor fragments was considered to be suitable because the propensity of a peptide or a protein to adopt a particular folding is primarily related to the amino acid sequence. Moreover, previous 3D conformational studies of the 7TM domain proteins, bovine rhodopsin (*33*) and bacteriorhodopsin (*34*, *35*) as well as those of 4TM domain proteins such as myohemerythrin (*36*) showed that the structural fragments of a receptor frequently adopt a geometry very similar to that found in the native molecule. As a matter of fact, this approach was also used before to study the structural domains of some GPCRs in the absence of X-ray diffraction data (*37*−*41*).

With CD analyses, it was observed that TM-IV adopts a stabilized α-helix conformation when dissolved in a medium containing organic solvents or cosolutes able to form micelles. Hence, the stability of this helical structure is rather high and present in a large variety of solvent conditions, including neat MeOH, aqueous fluorinated solvents, and micelle conditions. Using DICHROPROT, an estimate of the helix structure population was made from the CD spectra. Data suggested a content of 50% helical conformation, and this would correspond to approximately four turns of a helix. These results are supported by AGADIR, an algorithm designed for the prediction of helical structures, which proposed a high helicity for this transmembrane segment. Also, CD spectroscopy showed that EC-I exhibited a partial β-strand/random coil conformation when dissolved in an organic medium. Spectrum analysis using deconvolution suggested that about 10 residues are involved in the β-strand. These results are in agreement with the PHD prediction algorithm, which calculated that EC-I would contain two β-sheet segments corresponding to residues 111−118 and 122−126 of hUT, respectively. Moreover, AGADIR correlated the CD data and the PHD prediction method by establishing that the EC-I domain does not contain any α-helix arrangement.

The second extracellular loop of most GPCRs is usually the largest one and is considered to be highly susceptible to interactions with ligands. For EC-II, the CD results showed a combination of α-helix/random coil conformations, as those observed in solvent conditions including fluorinated alcohols (TFE, HFIP) or dodecylphosphocholine (DPC), a micelle producer. The deconvolution of the EC-II spectra suggested that the peptide molecule contains a α-helix consisting of 6−10 residues. This result is not in agreement with the estimate made with AGADIR, which predicted two α-helix domains located at the *N*- ($UT_{183-193}$) and *C*-termini ($UT_{205-210}$) of the fragment. In fact, those segments probably include a few residues of TM-IV and TM-V, which are causing the initiation of helical turns, because the exact *N*- and *C*-boundaries of the EC-II loop cannot be established with precision. Hence, it is probable that the helix geometry observed by CD for EC-II comes in part from the secondary structure adopted by both extremities of the receptor fragment. Because of the purported role of EC-II, particularly in the binding process, it is unlikely that this loop does not adopt a highly predominant conformation in the native receptor. Therefore, the absence of a prevalent secondary structure in EC-II suggests that key constraints are missing in the fragment. Extracellular loop II contains a cysteine residue (Cys^{199}) that is hypothesized to form a disulfide bridge with another cysteine (Cys^{123}) found in the first extracellular loop. This S−S bond was shown to be essential for the binding and activation of many GPCRs, such as the human VIP receptor (*42*) and the angiotensin II type 2 receptor (*43*). In the case of the EC-II of UT, we showed that the corresponding fragment is able to specifically recognize two agonists and one peptidic antagonist, thus demonstrating that the disulfide bridge is probably useful but not essential for the expression of the affinity. Nevertheless, the presence of such a covalent bond between EC-I and EC-II, which brings down EC-II closer to the cell membrane surface (*22*), is most likely a factor contributing to the stabilization of the folding of this receptor component. Furthermore, the neighboring of both loop boundaries, as produced in the native receptor by the anchoring of the EC-II extremities to transmembrane domains IV and V, respectively, could also be a critical driving force in inducing a stable molecular structure in EC-II. Nonetheless, although in its actual form only two to three turns of a helix are suggested for EC-II by the CD data, it is postulated that the helical structure is a requirement for ligand binding.

The CD spectrum of EC-III showed a pattern similar to that of EC-II. In an aqueous buffer, this peptide showed no specific structure. However, upon the addition of HFIP or micelle makers such as SDS or DPC, EC-III also exhibited some propensity to adopt a helical structure. This CD result is in agreement with the AGADIR algorithm, which proposes a helix folding involving about 4−9 residues, into segment UT (290−298), and corresponding to one to two turns. These would be approximately located in the second portion of the peptide sequence and would correspond to segment 290−298 of UT, where a purported site accessible for a hydrophobic interaction with the indole moiety of the Trp residue located in the cyclic core of U-II is found.

CONCLUSIONS

In line with previous studies carried out with known GPCRs that showed that the membrane domains of a receptor adopt frequently a geometry very similar to that found in the native molecule, we analyzed a number of structural characteristics and affinity properties of some urotensin-II receptor (UT) segments. Thus, using synthetic UT fragments related to the structural domains, we showed that EC loop II was able to recognize the ligands U-II, URP, and urantide, whereas EC loop III bound only to U-II and URP. These two fragments exhibited some helicity, which could be correlated to the affinity. Indeed, these binding properties were not shared with EC-I, a peptide in which a β-strand arrangement prevailed. Furthermore, the absence of binding of urantide, a peptide antagonist, strongly suggested that loop III would be involved in the signal transduction process. The specificity measured during the affinity assessment and the particular folding observed with the three extracellular loops showed that the strategy yielded data highlighting two key structural domains, EC-II and EC-III. Moreover, the results indicate that potent UT antagonists could be designed by producing high affinity ligands targeting extracellular loop II.

REFERENCES

1. Pearson, D., Shively, J. E., Clark, B. R., Geschwind, II, Barkley, M., Nishioka, R. S., and Bern, H. A. (1980) Urotensin II: a somatostatin-like peptide in the caudal neurosecretory system of fishes, *Proc. Natl. Acad. Sci. U.S.A. 77*, 5021−5024.
2. Bern, H. A., and Lederis, K. (1969) A reference preparation for the study of active substances in the caudal neurosecretory system of teleosts, *J. Endocrinol. 45*, Suppl. 11−12.
3. Conlon, J. M., Yano, K., Waugh, D., and Hazon, N. (1996) Distribution and molecular forms of urotensin II and its role in cardiovascular regulation in vertebrates, *J. Exp. Zool. 275*, 226−238.
4. Conlon, J. M., O'Harte, F., Smith, D. D., Tonon, M. C., and Vaudry, H. (1992) Isolation and primary structure of urotensin II from the brain of a tetrapod, the frog Rana ridibunda, *Biochem. Biophys. Res. Commun. 188*, 578−583.
5. Coulouarn, Y., Jegou, S., Tostivint, H., Vaudry, H., and Lihrmann, I. (1999) Cloning, sequence analysis and tissue distribution of the mouse and rat urotensin II precursors, *FEBS Lett. 457*, 28−32.
6. Conlon, J. M., Tostivint, H., and Vaudry, H. (1997) Somatostatin- and urotensin II-related peptides: molecular diversity and evolutionary perspectives, *Regul. Pept. 69*, 95−103.
7. Douglas, S. A., and Ohlstein, E. H. (2000) Human urotensin-II, the most potent mammalian vasoconstrictor identified to date, as a therapeutic target for the management of cardiovascular disease, *Trends Cardiovasc. Med. 10*, 229−237.
8. Camarda, V., Rizzi, A., Calo, G., Gendron, G., Perron, S. I., Kostenis, E., Zamboni, P., Mascoli, F., and Regoli, D. (2002) Effects of human urotensin II in isolated vessels of various species; comparison with other vasoactive agents, *Naunyn−Schmiedeberg's Arch. Pharmacol. 365*, 141−149.
9. Douglas, S. A., Sulpizio, A. C., Piercy, V., Sarau, H. M., Ames, R. S., Aiyar, N. V., Ohlstein, E. H., and Willette, R. N. (2000) Differential vasoconstrictor activity of human urotensin-II in vascular tissue isolated from the rat, mouse, dog, pig, marmoset and cynomolgus monkey, *Br. J. Pharmacol. 131*, 1262−1274.
10. Behm, D. J., Harrison, S. M., Ao, Z., Maniscalco, K., Pickering, S. J., Grau, E. V., Woods, T. N., Coatney, R. W., Doe, C. P., Willette, R. N., Johns, D. G., and Douglas, S. A. (2003) Deletion of the UT receptor gene results in the selective loss of urotensin-II contractile activity in aortae isolated from UT receptor knockout mice, *Br. J. Pharmacol. 139*, 464−472.
11. Ames, R. S., Sarau, H. M., Chambers, J. K., Willette, R. N., Aiyar, N. V., Romanic, A. M., Louden, C. S., Foley, J. J., Sauermelch, C. F., Coatney, R. W., Ao, Z., Disa, J., Holmes, S. D., Stadel, J. M., Martin, J. D., Liu, W. S., Glover, G. I., Wilson, S., McNulty, D. E., Ellis, C. E., Elshourbagy, N. A., Shabon, U., Trill, J. J., Hay, D. W., Ohlstein, E. H., Bergsma, D. J., and Douglas, S. A. (1999) Human urotensin-II is a potent vasoconstrictor and agonist for the orphan receptor GPR14, *Nature 401*, 282−286.
12. Liu, Q., Pong, S. S., Zeng, Z., Zhang, Q., Howard, A. D., Williams, D. L., Jr., Davidoff, M., Wang, R., Austin, C. P., McDonald, T. P., Bai, C., George, S. R., Evans, J. F., and Caskey, C. T. (1999) Identification of urotensin II as the endogenous ligand for the orphan G-protein-coupled receptor GPR14, *Biochem. Biophys. Res. Commun. 266*, 174−178.
13. Marchese, A., Heiber, M., Nguyen, T., Heng, H. H., Saldivia, V. R., Cheng, R., Murphy, P. M., Tsui, L. C., Shi, X., Gregor, P., and et al. (1995) Cloning and chromosomal mapping of three novel genes, GPR9, GPR10, and GPR14, encoding receptors related to interleukin 8, neuropeptide Y, and somatostatin receptors, *Genomics 29*, 335−344.
14. Maguire, J. J., Kuc, R. E., and Davenport, A. P. (2000) Orphan-receptor ligand human urotensin II: receptor localization in human tissues and comparison of vasoconstrictor responses with endothelin-1, *Br. J. Pharmacol. 131*, 441−446.
15. Brkovic, A., Hattenberger, A., Kostenis, E., Klabunde, T., Flohr, S., Kurz, M., Bourgault, S., and Fournier, A. (2003) Functional and binding characterizations of urotensin II-related peptides in human and rat urotensin II-receptor assay, *J. Pharmacol. Exp. Ther. 306*, 1200−1209.
16. Flohr, S., Kurz, M., Kostenis, E., Brkovich, A., Fournier, A., and Klabunde, T. (2002) Identification of nonpeptidic urotensin II receptor antagonists by virtual screening based on a pharmacophore model derived from structure−activity relationships and nuclear magnetic resonance studies on urotensin II, *J. Med. Chem. 45*, 1799−1805.
17. Grieco, P., Rovero, P., and Novellino, E. (2004) Recent structure−activity studies of the peptide hormone urotensin-II, a potent vasoconstrictor, *Curr. Med. Chem. 11*, 969−979.
18. Labarrere, P., Chatenet, D., Leprince, J., Marionneau, C., Loirand, G., Tonon, M. C., Dubessy, C., Scalbert, E., Pfeiffer, B., Renard, P., Calas, B., Pacaud, P., and Vaudry, H. (2003) Structure−activity relationships of human urotensin II and related analogues on rat aortic ring contraction, *J. Enzyme Inhib. Med. Chem. 18*, 77−88.
19. Kinney, W. A., Almond Jr, H. R., Qi, J., Smith, C. E., Santulli, R. J., de Garavilla, L., Andrade-Gordon, P., Cho, D. S., Everson, A. M., Feinstein, M. A., Leung, P. A., and Maryanoff, B. E. (2002) Structure−function analysis of urotensin II and its use in the construction of a ligand−receptor working model, *Angew. Chem., Int. Ed. 41*, 2940−2944.
20. Bhaskaran, R., Arunkumar, A. I., and Yu, C. (1994) NMR and dynamical simulated annealing studies on the solution conformation of urotensin II, *Biochim. Biophys. Acta 1199*, 115−122.
21. Chatenet, D., Dubessy, C., Leprince, J., Boularan, C., Carlier, L., Segalas-Milazzo, I., Guilhaudis, L., Oulyadi, H., Davoust, D., Scalbert, E., Pfeiffer, B., Renard, P., Tonon, M. C., Lihrmann, I., Pacaud, P., and Vaudry, H. (2004) Structure−activity relationships and structural conformation of a novel urotensin II-related peptide, *Peptides 25*, 1819−1830.
22. Lavecchia, A., Cosconati, S., and Novellino, E. (2005) Architecture of the human urotensin II receptor: comparison of the binding domains of peptide and non-peptide urotensin II agonists, *J. Med. Chem. 48*, 2480−2492.
23. Boucard, A. A., Sauve, S. S., Guillemette, G., Escher, E., and Leduc, R. (2003) Photolabeling the rat urotensin II/GPR14 receptor identifies a ligand-binding site in the fourth transmembrane domain, *Biochem. J. 370*, 829−838.

24. Kyte, J., and Doolittle, R. F. (1982) A simple method for displaying the hydropathic character of a protein., *J. Mol. Biol. 157*, 105−132.
25. Tusnady, G. E., and Simon, I. (2001) The HMMTOP transmembrane topology prediction server, *Bioinformatics 17*, 849−850.
26. Munoz, V., and Serrano, L. (1997) Development of the multiple sequence approximation within the AGADIR model of alpha-helix formation: comparison with Zimm-Bragg and Lifson-Roig formalisms, *Biopolymers 41*, 495−509.
27. Rost, B., and Sander, C. (1994) Combining evolutionary information and neural networks to predict protein secondary structure, *Proteins 19*, 55−72.
28. Cserzo, M., Eisenhaber, F., Eisenhaber, B., and Simon, I. (2002) On filtering false positive transmembrane protein predictions, *Protein Eng. 15*, 745−752.
29. Sonnhammer, E. L., von Heijne, G., and Krogh, A. (1998) A hidden Markov model for predicting transmembrane helices in protein sequences, *Proc. Int. Conf. Intell. Syst. Mol. Biol. 6th 6*, 175−182.
30. Yin, D., Gavi, S., Wang, H. Y., and Malbon, C. C. (2004) Probing receptor structure/function with chimeric G-protein-coupled receptors, *Mol. Pharmacol. 65*, 1323−1332.
31. Grieco, P., Carotenuto, A., Campiglia, P., Zampelli, E., Patacchini, R., Maggi, C. A., Novellino, E., and Rovero, P. (2002) A new, potent urotensin II receptor peptide agonist containing a Pen residue at the disulfide bridge, *J. Med. Chem. 45*, 4391−4394.
32. Patacchini, R., Santicioli, P., Giuliani, S., Grieco, P., Novellino, E., Rovero, P., and Maggi, C. A. (2003) Urantide: an ultrapotent urotensin II antagonist peptide in the rat aorta, *Br. J. Pharmacol. 140*, 1155−1158.
33. Yeagle, P. L., Danis, C., Choi, G., Alderfer, J. L., and Albert, A. D. (2000) Three-dimensional structure of the seventh transmembrane helical domain of the G-protein receptor, rhodopsin, *Mol. Vis. 6*, 125−131.
34. Katragadda, M., Alderfer, J. L., and Yeagle, P. L. (2000) Solution structure of the loops of bacteriorhodopsin closely resembles the crystal structure, *Biochim. Biophys. Acta 1466*, 1−6.
35. Nikiforovich, G. V., Galaktionov, S., Balodis, J., and Marshall, G. R. (2001) Novel approach to computer modeling of seven-helical transmembrane proteins: current progress in the test case of bacteriorhodopsin, *Acta Biochim. Pol. 48*, 53−64.
36. Dyson, H. J., Merutka, G., Waltho, J. P., Lerner, R. A., and Wright, P. E. (1992) Folding of peptide fragments comprising the complete sequence of proteins. Models for initiation of protein folding. I. Myohemerythrin, *J. Mol. Biol. 226*, 795−817.
37. Ruan, K. H., So, S. P., Wu, J., Li, D., Huang, A., and Kung, J. (2001) Solution structure of the second extracellular loop of human thromboxane A2 receptor, *Biochemistry 40*, 275−280.
38. Ulfers, A. L., Piserchio, A., and Mierke, D. F. (2002) Extracellular domains of the neurokinin-1 receptor: structural characterization and interactions with substance P, *Biopolymers 66*, 339−349.
39. Demene, H., Granier, S., Muller, D., Guillon, G., Dufour, M. N., Delsuc, M. A., Hibert, M., Pascal, R., and Mendre, C. (2003) Active peptidic mimics of the second intracellular loop of the V(1A) vasopressin receptor are structurally related to the second intracellular rhodopsin loop: a combined 1H NMR and biochemical study, *Biochemistry 42*, 8204−8213.
40. Giragossian, C., and Mierke, D. F. (2001) Intermolecular interactions between cholecystokinin-8 and the third extracellular loop of the cholecystokinin A receptor, *Biochemistry 40*, 3804−3809.
41. Zhang, L., DeHaven, R. N., and Goodman, M. (2002) NMR and modeling studies of a synthetic extracellular loop II of the kappa opioid receptor in a DPC micelle, *Biochemistry 41*, 61−68.
42. Knudsen, S. M., Tams, J. W., Wulff, B. S., and Fahrenkrug, J. (1997) A disulfide bond between conserved cysteines in the extracellular loops of the human VIP receptor is required for binding and activation, *FEBS Lett. 412*, 141−143.
43. Heerding, J. N., Hines, J., Fluharty, S. J., and Yee, D. K. (2001) Identification and function of disulfide bridges in the extracellular domains of the angiotensin II type 2 receptor, *Biochemistry 40*, 8369−8377.

BI060190B